Astronomy & Astrophysics

Searching for multiple stellar populations in the massive, old open cluster Berkeley 39[⋆,⋆⋆]

A. Bragaglia[1], R. G. Gratton[2], E. Carretta[1], V. D'Orazi[3,4], C. Sneden[5], and S. Lucatello[2]

[1] INAF – Osservatorio Astronomico di Bologna, via Ranzani 1, 40127 Bologna, Italy
  e-mail: angela.bragaglia@oabo.inaf.it
[2] INAF – Osservatorio Astronomico di Padova, Vicolo dell'Osservatorio 5, 35122 Padova, Italy
[3] Department of Physics and Astronomy, Macquarie University, Balaclava Rd, North Ryde, NSW 2109, Australia
[4] Monash Centre for Astrophysics, School of Mathematical Sciences, Building 28, Monash University, VIC 3800, Australia
[5] Department of Astronomy and McDonald Observatory, The University of Texas, Austin, TX 78712, USA

ABSTRACT

The most massive star clusters include several generations of stars with a different chemical composition (mainly revealed by an Na-O anti-correlation) while low-mass star clusters appear to be chemically homogeneous. We are investigating the chemical composition of several clusters with masses of a few 10^4 $M_\odot$ to establish the lower mass limit for the multiple stellar population phenomenon. Using VLT/FLAMES spectra we determine abundances of Fe, O, Na, and several other elements (α, Fe-peak, and neutron-capture elements) in the old open cluster Berkeley 39. This is a massive open cluster: $M \sim 10^4$ $M_\odot$, approximately at the border between small globular clusters and large open clusters. Our sample size of about 30 stars is one of the largest studied for abundances in any open cluster to date, and will be useful to determine improved cluster parameters, such as age, distance, and reddening when coupled with precise, well-calibrated photometry. We find that Berkeley 39 is slightly metal-poor, $\langle$[Fe/H]$\rangle = -0.20$, in agreement with previous studies of this cluster. More importantly, we do not detect any star-to-star variation in the abundances of Fe, O, and Na within quite stringent upper limits. The rms scatter is 0.04, 0.10, and 0.05 dex for Fe, O, and Na, respectively. This small spread can be entirely explained by the noise in the spectra and by uncertainties in the atmospheric parameters. We conclude that Berkeley 39 is a single-population cluster.

Key words. stars: abundances – open clusters and associations: general – open clusters and associations: individual: Berkeley 39 – stars: atmospheres

1. Introduction

Most, perhaps all, Galactic globular clusters (GCs) host multiple stellar populations that can be identified by variations of Na and O abundances (e.g, Carretta et al. 2010, and references therein), which are anti-correlated with each other (see e.g., Gratton et al. 2004, 2012, for recent reviews). On the other hand, Na-rich and O-poor stars that are common in GCs are rare among field stars (Carretta et al.) and are possibly absent from open clusters (OCs, see e.g., de Silva et al. 2009). A similar result is obtained for other light elements, such as C and N, see e.g., Martell & Smith (2009), Martell & Grebel (2010). The onset of the mechanism that leads to the multiple stellar population phenomenon is tied to the dynamics of the star formation process and has in turn to depend on many variables such as age, metallicity, total mass, and probably also on the environment (e.g., position in the Galaxy or in a smaller galaxy) where the cluster formed. According to Carretta et al. (2010), however, there seems to be a minimum (present-day) threshold mass of about a few 10^4 $M_\odot$, as shown in Fig. 1 (an updated version of the M_V-age plot originally presented in Carretta et al. 2010).

Unfortunately, few clusters with masses close to this threshold value have been surveyed extensively enough to show

whether they really have Na and O abundance variations (see e.g., Carretta et al. 2010; Bragaglia 2012). Two GCs in this mass interval, Ter 7 and Pal 1 (Fig. 1) seem to lack these variations; however, only a handful of stars in each of them has been studied (Tautvaišienė et al. 2004; Sbordone et al. 2005, 2007; Cohen 2004). Another case seems to be Rup 106 (Geisler & Villanova 2012), at a higher present-day mass. A possible case for variations in the abundances of these elements has recently been made for the massive old open cluster NGC 6791 (Geisler et al. 2012, but see the conflicting conclusion reached by our group, Bragaglia et al., in prep.).

Observation of a larger sample of clusters is required, with the same kind of large samples we obtained for more than 20 GCs using the multi-object, high-resolution spectrograph VLT/FLAMES (see e.g., Carretta et al. 2009a,b). We have started systematic observations of clusters in this transition region, including both the most massive metal-rich disc open clusters and the faint end of the mass distribution of metal-poor globular clusters. This approach may help to understand if the only factor at play is mass (remembering of course that M_V measures the present-day mass, not directly the original one), or if other factors, such as the environment in which the clusters formed, have to be considered.

In this paper we present results for the OC Berkeley 39, an old (about 6 Gyr, Kassis et al. 1997, and Sect. 2.1) massive OC ($M_V = -4.28$, Lata et al. 2002, indicating a mass of $\sim 2 \times 10^4$ $M_\odot$, see Fig. 1). Be 39 is located in the outer part of the disc, at about

---
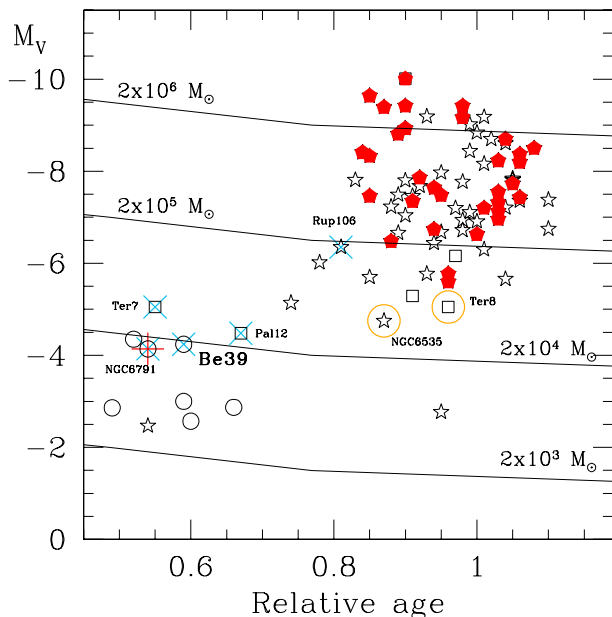
Fig. 1. Relative age parameter vs. absolute magnitude M_V for globular and old open clusters. Red filled symbols are GCs where the Na-O anti-correlation has been observed; open star symbols and open squares mark MW and Sagittarius GCs, respectively, for which not enough data are available; open circles are old open clusters (data from Lata et al. 2002). Finally, light blue crosses indicate several clusters that do not show evidence of Na-O anti-correlation: two GC members of Sagittarius dSph, one of the main body (Ter 7) and one of the stream (Pal 12); the new entry Rup 106; and two massive, old OCs, Be 39 and NGC 6791 (the latter indicated also in red, since its situation is still not completely assessed). Two orange, large circles indicate the other GCs of our project. Superimposed are lines of constant mass (light solid lines, see Bellazzini et al. 2008).

11 kpc from the Galactic centre (see Friel et al. 2010). Friel et al. determined the chemical composition of this cluster from high-resolution spectra of four red giants. These authors showed that this cluster is slightly metal-poor ([Fe/H] = -0.21 ± 0.01), which agrees very well with the metallicities of other clusters at similar Galactocentric distances (see their Fig. 3). Friel et al. obtained very consistent results from their four stars. However, their sample is too small to exclude a significant spread in abundances in the cluster, as would be expected from the multiple population phenomenon. Extant photometric data are not sufficiently accurate to shed light on this question (see Sect. 2.1). Chemical inhomogenieties in Be 39 cannot be ruled out at present. Therefore we included Be 39 in our survey, and obtained abundances from high-resolution spectra for several tens of member stars, a substantial fraction of the evolved population of this cluster.

While the spectral regions of our data were optimised to discuss the Na-O anti-correlation, our spectra have a wider interest. Open clusters are good tracers of the properties of the disc of our Galaxy, see e.g., Friel (1995); Bragaglia & Tosi (2006); Yong et al. (2012) and references therein. Notwithstanding many observational efforts, only a fraction of the known Galactic OCs (about 2000, according to the catalogue in Dias et al. 2002, and its updates) have been observed with high-resolution spectroscopy. Searching the literature, we found only about 80 with an age older than 100 Myr (see Sect. 4) and in general only a handful of stars were observed in each of them. If one aims to investigate the history of the Galactic disc (formation and evolution), the old clusters are very important; our observations provide further, improved information on one of the few very

old OCs. The large sample of stars is also very useful, because it permits us to put stringent constraints to the internal abundance homogeneity, something that is relevant for the cluster formation mechanisms.

The paper is organized as follows: in Sect. 2 we present the basic data for this cluster, the selection of stars to be observed, and the observations themselves. In Sect. 3 we describe the analysis method; a critical point is the derivation of accurate atmospheric parameters. In Sect. 4 we present and discuss the results of our analysis. Section 5 contains the summary and conclusions.

2. Observations

2.1. Photometry and cluster parameters

Photometric observations for Be 39 have been used to study its variable stars and to determine the cluster parameters (see e.g., Kaluzny & Richtler 1989; Kassis et al. 1997); a summary of past results can be found in Friel et al. (2010). Of the publicly available optical photometry, Kaluzny & Richtler (1989) collected B, V data on a small field of view (4.5×7.2 arcmin^2) while Kassis et al. (1997) provided B, V, I photometry on a 14.7×14.7 arcmin^2 area, better suited to the FLAMES spectrograph field (25′ in diameter, Pasquini et al. 2002). We obtained the two photometric catalogues through the database WEBDA[1] and used the second set to select our targets (see Fig. 2).

In our series of papers on the Na-O anti-correlation in GCs we used atmospheric parameters directly derived from the photometry, so we checked if it was possible to do the same for Be 39 as well. Unfortunately, the two photometric data sets are not identical; they show an average difference of -0.02 (rms = 0.07) mag in V and $+0.06$ (rms = 0.10) mag in B (in the sense Kassis et al. minus Kaluzny & Richtler) based on about 730 stars in common. This could seem a minor effect, but a difference of about 0.07–0.08 mag in $B - V$ means a large difference in stellar effective temperatures in Be 39. Furthermore, the largest discrepancies between the two sets are found also among the brightest stars, especially the red giant branch (RGB) and red clump (RC) ones. We were unable to unequivocally establish which, if either, of the two photometric sets is the best calibrated, so we adopted the Kassis et al. (1997) one because it is available over a larger field of view. However, we manually adjusted a few values for stars that are radial-velocity (RV) members of the cluster but have magnitudes and colours that are discrepant from the evolutionary sequences (see Sect. 3.1) in one of the CMDs.

We also re-determined the cluster parameters, using the Padova isochrones (Marigo et al. 2008) retrieved from the interactive database http://stev.oapd.inaf.it/cgi-bin/cmd at the metallicity derived by Friel et al. (2010), i.e., [Fe/H] = -0.20. Figure 2 (right panel) shows the result; the age is between 5.5 and 7 Gyr, with a best-guess age of about 6 Gyr. The distance modulus is $(m - M)_0 = 12.94$, and the reddening is $E(B - V) = 0.17$, slightly higher than found in previous studies (but consistent, considering the relatively large uncertainties in the photometric data). These values were used to determine effective temperatures and surface gravities of the programme stars (Sect. 3.1). Note however from the figure that RGB stars do not define a narrow sequence; this could be partly because of undetected binaries, but could also indicate differential reddening and/or uncertain photometric values.

We could not locate Strömgren colours for Be 39, which could have been used to test the uni- or multi-population nature

---

[1] The OC database is at
http://www.univie.ac.at/webda/webda.html
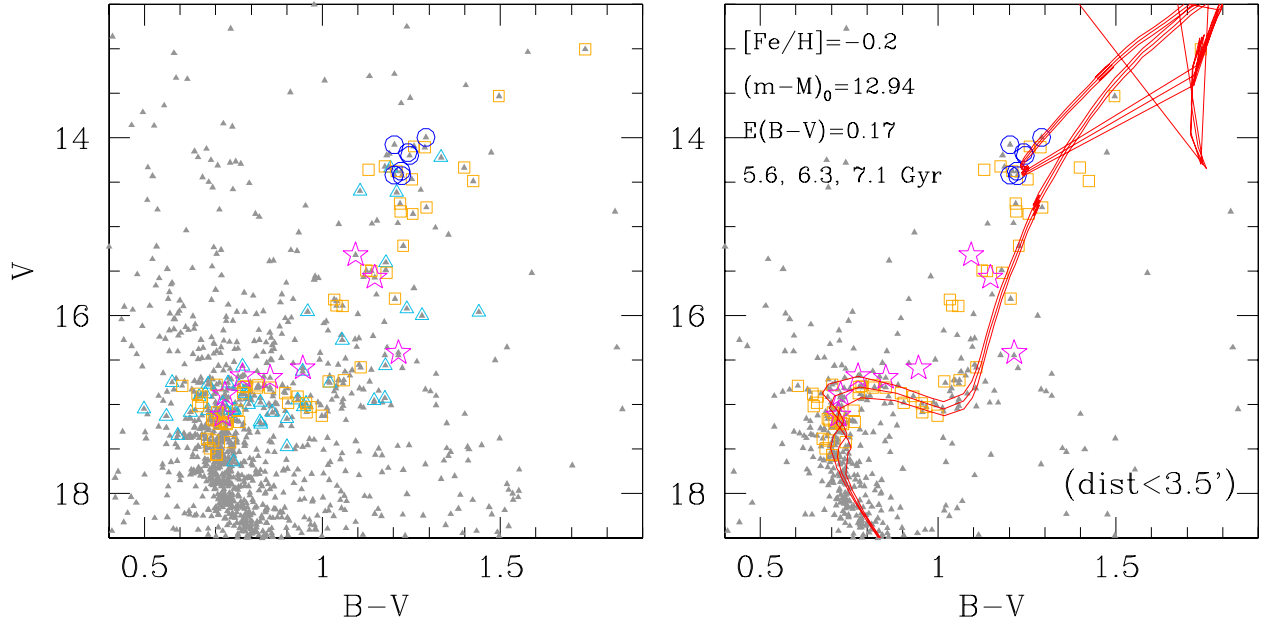
Fig. 2. *Left*: CMD for Be 39 (Kassis et al. 1997) with observed stars indicated by different symbols: UVES target (blue circles), GIRAFFE targets (orange squares for members, cyan triangles non-members), binaries (magenta stars). *Right*: CMD for the inner 3.5 arcmin, with observed member stars indicated by larger symbols and three isochrones shown. The parameters used for the fit are indicated.

of the cluster, as discussed on empirical grounds by Carretta et al. (2011) and on theoretical ones by Sbordone et al. (2011). The latter paper also considered the more usually available Johnson-Cousins bands; however, as we have noted, existing broadband photometry in those filters is not sufficiently precise for this goal.

2.2. FLAMES data

We obtained six exposures of Be 39 with the multi-object spectrograph VLT/FLAMES, as in our previous studies on the Na-O anti-correlations in clusters. The observations were obtained in service mode and were spaced in time (see Table 1) to search for RV variations that would indicate the presence of binary systems. We used the UVES 580nm setup ($\lambda\lambda \simeq 4800-6800$ Å) and the GIRAFFE high-resolution grating HR13, which contains the [O I] line at 6300 Å and the Na I doublet at 6154–6160 Å.

We selected Be 39 candidates using available information on RV from Friel et al. (2002) and Friel et al. (2010) to help selecting only probable cluster members. All chosen targets are free from neighbours: they have no other stars closer than 3″ (or 2″ if they are at least 2 mag fainter than the desired candidates). As shown in Fig. 2, we selected stars on the RC, or close to it, for the UVES fibres; only one configuration was prepared, so we have seven stars observed at high-resolution ($R \simeq 45\,000$), with the eighth fibre used for sky subtraction. The GIRAFFE fibres (at $R \simeq 22\,500$) were allocated to other RC and RGB objects and to stars on the subgiant branch (SGB) and the turn-off (TO) of the main sequence; 16 fibres were used for sky correction. For the SGB and TO stars the spectral region is not ideal, since the [O I] line is too weak to be measured. The Na I features of these stars still could be used to search for a possible Na abundance spread. However, the main targets of our observations are RGB and RC stars, for which Na and O can be measured; the most interesting information provided by fainter stars is their RV (i.e., membership). Information on all observed stars can be found in Table 2; we give the ID in the Kassis et al. (1997) catalogue, the

Table 1. Log of the observations.

OB	UT date (Y-M-D)	UT$_{init}$ (h:m:s)	Exp time (s)	Airmass	Seeing (arcsec)
A	2010-12-10	06:26:33.886	2345	1.085	0.51
B	2010-12-10	07:19:18.192	2450	1.064	0.48
C	2010-12-13	05:07:19.888	2450	1.205	0.66
D	2011-01-26	04:14:19.507	2450	1.064	0.55
E	2011-02-27	02:59:58.770	2450	1.096	1.26
F	2011-03-06	02:35:28.955	2345	1.100	1.30

ID in WEBDA, equatorial coordinates, V, $B-V$ and $V-I$ colours (with a flag indicating stars corrected as described above), and the heliocentric RV.

The spectra were reduced (bias and flat field corrected, 1-D extracted, and wavelength-calibrated) by the ESO personnel. We applied sky subtraction and division by an observed early-type star (UVES) or a synthetic spectrum (computed at the GIRAFFE spectral resolution) to correct for telluric features near the [O I] line, using the IRAF[2] routine *telluric*. The latter correction was applied only to the UVES and bright GIRAFFE samples (RC, RGB stars), since this [O I] line is not usable in the warmer faint GIRAFFE stars (SGB and TO). We measured the individual RVs using *rvidlines* in IRAF and shifted all spectra to zero velocity before combining them. The UVES final spectra have signal-to-noise ratio (S/N) in the range 100–170. The S/N ratios (computed on small continuum regions) of GIRAFFE spectra of RC stars are in the range 150–210; of RGB stars are generally between 100 and 200, and those of SGB and TO stars are 25–70. Values for individual stars are listed in Table 2. A portion of the UVES spectra showing the Na I lines region is shown in Fig. 3.

---

[2] IRAF is distributed by the National Optical Astronomical Observatory, which are operated by the Association of Universities for Research in Astronomy, under contract with the National Science Foundation.
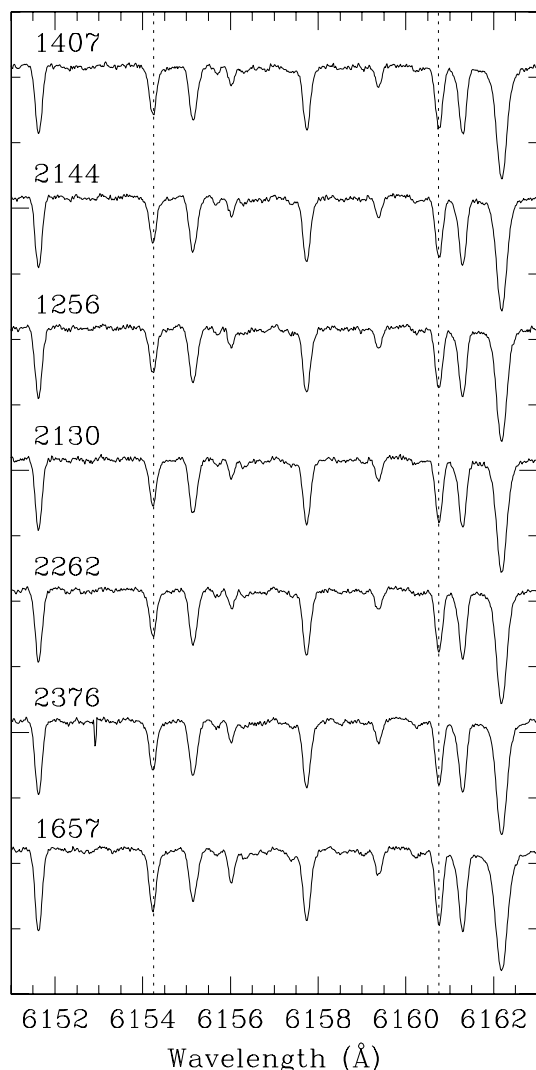
Fig. 3. Portion of the UVES spectra in the Na I lines region; the two Na lines are indicated by the dotted lines. The normalised spectra are offset for clarity and are plotted in order of decreasing T_{eff}, with the RGB star at the bottom. The Na and all other lines are practically identical in all stars, with only a small difference between the RGB and the RC ones.

Fig. 4. Histogram of all RVs for the FLAMES spectra (red, open histogram) and for the Besançon model (Robin et al. 2003) in the direction of Be 39, on the same area of the Kassis et al. (1997) data and normalised to the number of our stars (filled, grey histogram).
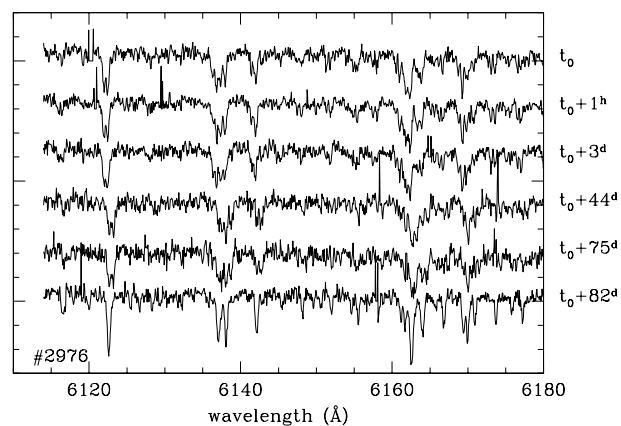
Fig. 5. Six spectra obtained for star #2976, a binary near the base of the RGB. The right axis indicates the time since the first observation.

The cluster average RV was computed separately for UVES and GIRAFFE spectra. We found $\langle RV_{\mathrm{UVES}} \rangle = 57.35$ (rms = 0.85) km s^{-1} and $\langle RV_{\mathrm{GIRAFFE}} \rangle = 58.21$ (rms = 1.62) km s^{-1}. We assume that all stars within $\pm 3\sigma$ from the average are cluster members, with some more dubious cases indicated in Table 2. Both these values compare well to RV = 58.65 (rms = 2.34) km s^{-1} (Friel et al. 2010) and RV = 55.0 (rms = 2.9) km s^{-1} (Frinchaboy et al. 2006). Figure 4 shows the RV distribution of our stars and compares it to the expected distribution of field star velocities, according to the Besançon model (Robin et al. 2003). Be 39 stands out conspicuously and fewer than about ten field stars have RVs similar to the cluster one.

After pruning the sample using RVs we found a total of 67 possible single member stars. All seven UVES stars are RV members; of the GIRAFFE stars, 60 are possible members, eight are binary systems, and 43 are non-members. This is one of the largest sample of spectroscopically studied stars in OCs.

While measuring the RVs we found a few stars with discrepant values at different observation times, which is indicative of binary systems. On closer inspection, some of them also displayed changes in spectrum appearance; an example is shown in Fig. 5. There is also a suggestion, combining our RVs with those of Friel et al. (2010, see Sect. 4.2), that one of the UVES and one of the GIRAFFE targets may be binary. If all these systems are members, this indicates a binary fraction of 10/75 or 13%. This is only a lower limit and it perfectly conforms to the fraction of binaries usually found in OCs from photometry (see e.g., Bragaglia & Tosi 2006).

3. Analysis

3.1. Atmospheric parameters

For this cluster we cannot apply the same procedure as we adopted for the GC survey (Carretta et al. 2009a,b). First, we saw that the photometry alone cannot guarantee atmospheric parameters with the required precision (at least, not for all stars). Second, we cannot use the IR K magnitude as we have
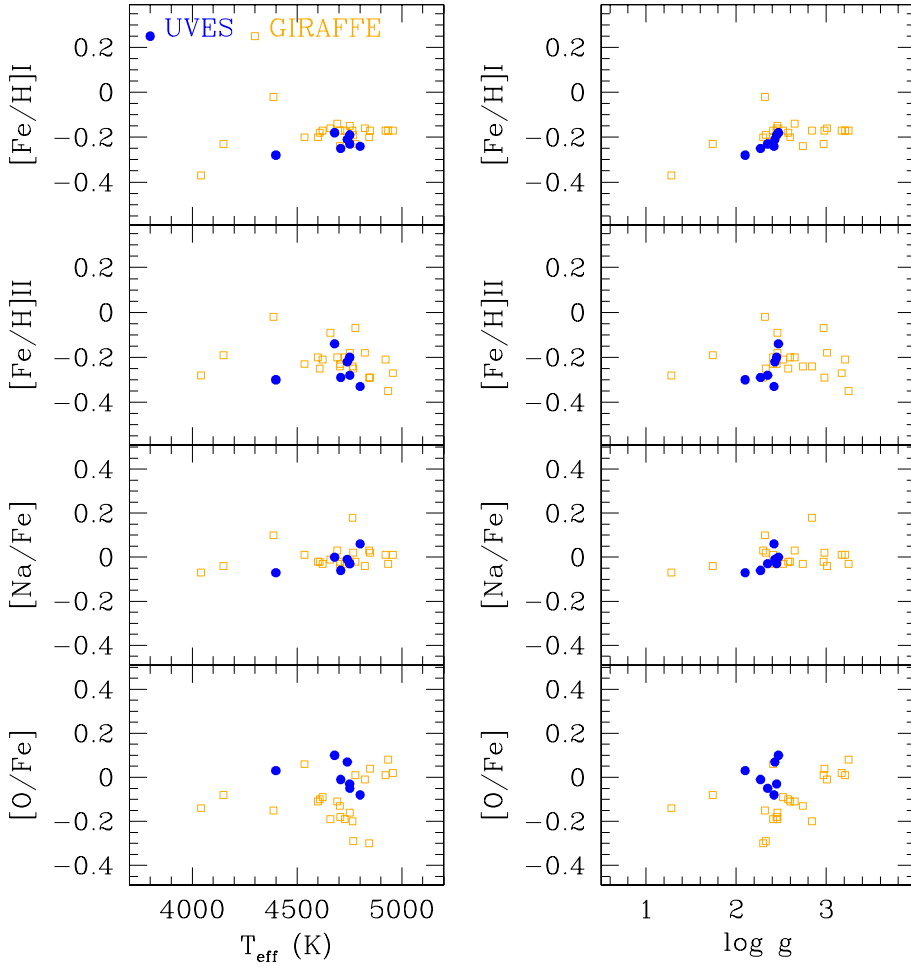
Fig. 6. Run of Fe I, Fe II, Na, and O with $T_{\rm eff}$ and $\log g$ for stars on the RGB and RC. Filled blue symbols are for UVES, open orange squares for GIRAFFE targets.

previously done for other clusters to determine the temperature from the $V - K$ colour. Our sample does not only include bright stars for which the 2MASS photometry would be precise enough, but also faint stars for which it would be unreliable. We could potentially infer false inhomogeneities were we to use this colour. On the other hand, B, V, and I photometry accurate enough (apart from the mismatches discussed in Sect. 2.1) is available for all targets. We therefore opted for temperatures derived from $B - V$ and $V - I$ as input values.

We used the reddening and distance modulus derived above, adopting $E(V - I) = 1.3E(B - V)$, $A_V = 3.1E(B - V)$, and 4.75 as bolometric magnitude of the Sun. We used the colour-temperature relations of Ramírez & Meléndez (2005) to find $T_{\rm eff}$, and averaged the values obtained from $B - V$ and $V - I$. The gravity was derived as in previous papers following the relations of Alonso et al. (1999) for the bolometric correction and a mass of 1.15 $M_\odot$, as deduced from the isochrones. Average photometric $T_{\rm eff}$ and $\log g$ values were computed, weighting more those obtained from the original colours than the "corrected" ones (see Sect. 2.1).

These $T_{\rm eff}$'s and $\log g$'s were used to derive first-pass iron abundances for all stars in our sample. The microturbulent velocities $v_{\rm t}$ were obtained from the relation $v_{\rm t} = -0.322 \log g + 2.22$ (Gratton et al. 1996). Adopting this relation, only very weak trends in the relation between abundances from Fe neutral lines and expected line strength (see Magain 1984) were apparent, with negligible effects on the abundances. We then computed the $T_{\rm eff}$ and $\log g$ values required to satisfy the excitation and ionisation equilibria (we recall, however, that there are only three

useful Fe II lines in the GIRAFFE HR13 wavelength range). The final adopted parameters are the average of the spectroscopic and photometric ones. Metallicities for all stars were then obtained with model atmospheres interpolated in the Kurucz (1993) grid of model atmospheres (without convective overshooting) with atmospheric parameters whose abundance matches that derived from Fe I lines.

Temperature, gravity, microturbulent velocity, and Fe I and II are given in Table 3 for the UVES and Giraffe bright sample (RGB and RC stars). The run of iron abundances with $T_{\rm eff}$ and $\log g$ are shown in the upper panels of Fig. 6. These abundances do not display any significant trends with $T_{\rm eff}$ (left-hand panels) or $\log g$ (right-hand panels). The weak trend that is possibly presented by the lower gravity stars in the [Fe/H] I-$\log g$ plane is negligible in the context of the present paper and could be caused by a variety of sources, such as blends, continuum tracing, or inadequacy of the model atmospheres – all more noticeable at cooler temperatures. We note, however, that there seems to be a small offset between the mean iron abundances of UVES and GIRAFFE stars. This is most probably due to the combination of higher resolution (hence accuracy in equivalent width, EW, measurement, see next section) and higher S/N for the UVES spectra. It is not worrisome, but in the next sections we will keep separate abundances from the two samples.

The values for the SGB and TO stars have larger errors and larger scatter because of the low S/N combined with the warm temperatures and the larger errors in the photometry. Furthermore, we could not derive O abundances for the faint sample: the stars are too warm to measure the [O I] line, but

Table 4. Sensitivity to errors.

Element	$T_{\rm eff}$ (K)	$\log g$ (dex)	[A/H] (dex)	$v_{\rm t}$ km s^{-1}	EW	Total error	Observed rms
		Δ parameter					
	100	0.30	0.10	0.2			
		Error					
	30	0.03	0.04	0.1			
Fe I	0.071	0.014	0.011	–0.093	0.013	0.053	0.049
Fe II	–0.164	0.046	0.026	0.043	0.036	0.066	0.067
O I	–0.058	0.114	0.027	0.087	0.085	0.098	0.119
Na I	0.004	–0.025	–0.015	0.059	0.052	0.060	0.050
Mg I	–0.032	–0.008	–0.007	0.071	0.053	0.065	0.066
Al I	–0.004	–0.019	–0.013	0.069	0.054	0.064	0.025
Si I	–0.101	0.033	0.010	0.061	0.047	0.064	0.065
Ca I	0.035	–0.063	–0.014	–0.008	0.019	0.024	0.093
Sc II	–0.087	0.118	0.025	0.028	0.053	0.063	0.060
Ti I	0.079	–0.020	–0.021	0.003	0.036	0.044	0.053
Ti II	–0.103	0.120	0.023	0.074	0.106	0.117	0.052
V I	0.096	–0.012	–0.019	0.030	0.023	0.041	0.129
Cr I	0.091	–0.008	–0.024	0.011	0.087	0.092	0.150
Mn I	0.031	–0.052	–0.001	–0.039	0.044	0.050	0.021
Co I	–0.027	0.036	0.008	0.062	0.090	0.096	
Ni I	–0.037	0.040	0.007	0.033	0.019	0.028	0.045
Ba II	–0.046	0.063	0.033	–0.084	0.046	0.066	0.120

not warm enough for the triplet at 6155–6158 Å. While we proceeded with a preliminary analysis also for the faint sample, we eventually decided to discard these stars and keep only the bright sample, for which our conclusions are sounder.

3.2. Equivalent widths, sensitivity, and errors

We measured EWs with the software package Rosa (Gratton 1988), as described in Bragaglia et al. (2001). We adopted the same automatic procedure to define the local continuum around each line as in previous papers, but we did not correct the GIRAFFE EWs to the UVES system because we did not have any star in common. Small differences between the two sets of EWs related to the different resolution of the spectra may indeed exist, and explain the small differences in the abundances. The EWs of the member stars are made available only through the CDS.

To evaluate the sensitivity of the derived abundances to the adopted atmospheric parameters we repeated our abundance analysis by changing only one parameter each time. The amount of the variations in the atmospheric parameters and the resulting response in abundance changes of Fe, O, Na, and all elements measured (i.e., the sensitivities) are shown in Table 4. In the upper part of the same table we also give the error contributed by each parameter. The column labelled "total error" gives the total error expected from uncertainties in the atmospheric parameters and in the EWs, to be compared to the observed scatter in order to understand if we have a statistically significant variation in any of the elements. Note that for some elements (including Ca, V, and Ba) the observed scatter is larger than the observational errors. However, for various reasons errors may have been underestimated for these elements: lines of Ca and Ba are strong and saturated, and those of V are affected by strong HFS effects.

Errors in our measures are the following.

$T_{\rm eff}$: The errors in $T_{\rm eff}$ were derived by examining the rms of residuals along a quadratic $\log g - T_{\rm eff}$ relation for RGB stars

(after eliminating RC stars). This residual is 29 K, so we assume an error of ±30 K.

$\log g$: The error in $\log g$ is dominated by the errors in $T_{\rm eff}$ (30 K, yielding an error of 0.006 dex) and in photometry (given all the uncertainties noted in Sect. 2.1, we assumed 0.05 mag, yielding an error of 0.02 dex). This yields a total error of ±0.03 dex.

[A/H]: The error is not larger than the observed star-to-star scatter, i.e., ±0.04 dex.

$v_{\rm t}$: This is the dominant source of errors for iron. It was estimated by considering the star-to-star scatter of the trends of abundances with expected line strength: the error is 0.09 km s^{-1}. We assumed an error of ±0.10 km s^{-1}.

4. Results

Abundances of all elements were derived from EWs (and from synthetic spectra for O). Hyperfine splitting corrections were applied for Sc, V, and Mn. We used the same lines and line parameters as in the papers of the FLAMES GC survey (e.g., Carretta et al. 2009b), originally from Gratton et al. (2003). Reference solar abundances are explicitly given in Table 5.

The average values for all elements measured are presented in Table 5, separately for the UVES and GIRAFFE samples, given the diversity of resolution, wavelength coverage, and number of lines available in the two cases. For UVES the average was derived from seven stars; for GIRAFFE it is typically derived from 21 stars. As stated above, only the brighter sample was considered. Furthermore, star 11 was always excluded because is more that 3σ away from the cluster average velocity and its approximately solar metallicity is clearly higher than that of the other stars of Be 39.

Be 39 clearly is a homogeneous cluster: the star-to-star scatter is always explained by the errors expected from uncertainties in atmospheric parameters and EWs (see Tables 4 and 5). In particular, we find a mean metallicity [Fe/H] = −0.23 (rms = 0.04) from UVES and −0.18 (rms = 0.06) from GIRAFFE spectra. This agrees very well with Friel et al. (2010, see also Sect. 4.2). It is also in accord with metallicity expectations for clusters at Be 39's Galactocentric distance; the cluster lies at an $R_{\rm GC}$ of about 11 kpc, where OCs generally have sub-solar metallicity, as shown in Fig. 7. Interestingly, its $R_{\rm GC}$ is around the transition between inner and outer disc, where the metallicity gradient begins to flatten. This is a region where more clusters should be observed to better constrain the models of chemical evolution (e.g., Magrini et al. 2009; Friel et al. 2010). For the figure we selected only clusters older than 100 Myr and with metallicity derived by high-resolution spectra; the sample contains 79 old OCs. The picture is quite clear; we caution, however, that the parameters (age, distance, metallicity) have not been put on a homogeneous scale since this would be a great effort, completely outside the goal of the present paper (see e.g., Yong et al. 2012, for a recent work on the abundances and trends in the outer disc). We also confirm Friel et al.'s derivation of a mild overabundance of α-elements ([α/Fe] ≃ 0.1).

Elements Al, Ti II, and Mn could only be measured in the UVES spectra. It is unfortunate that we could not measure Al also for the GIRAFFE sample, since it is involved in the light elements (anti-)correlations and may show also very strong star-to-star variations (see, e.g., Carretta et al. 2012, for the GC NGC 6752). But the UVES results suggest that this is not the case for Be 39 (see Table 5).

Barium is the only neutron-capture element we measured. Its abundance was derived from three lines in the UVES spectra at
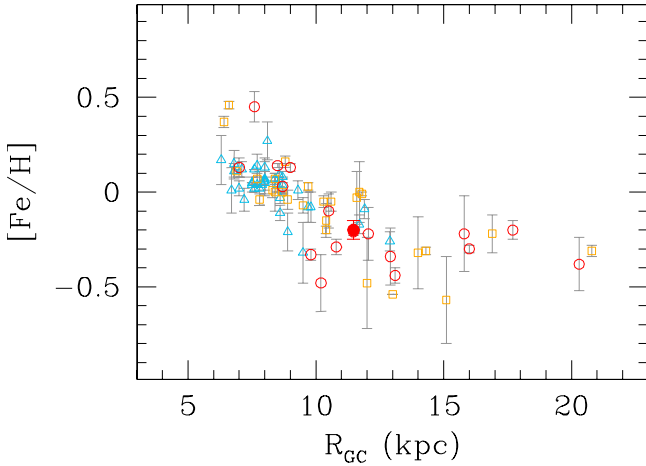
Fig. 7. Distribution of [Fe/H] with Galactocentric distance for OCs, colour-coded according to age (light blue triangles: age 0.1–1 Gyr; orange squares: age 1–4 Gyr; red circles: age older than 4 Gyr). [Fe/H] and errorbars are taken from the original literature sources. Be 39 is indicated with a filled red symbol.

Table 5. Average abundances for Be 39.

Element	Sun	Abu UVES	rms	Abu Giraffe	rms	Notes
[Fe/H] I	7.54	−0.23	0.04	−0.18	0.06	
[Fe/H] II	7.49	−0.19	0.05	−0.21	0.07	
[O/Fe] I	8.76	0.03	0.07	−0.08	0.11	
[Na/Fe] I	6.30	−0.02	0.04	−0.01	0.03	NLTE
[Mg/Fe] I	7.43	0.17	0.02	0.24	0.05	
[Al/Fe] I	6.40	0.02	0.03			
[Si/Fe] I	7.53	0.12	0.03	0.14	0.05	
[Ca/Fe] I	6.27	0.07	0.05	0.17	0.08	
[Sc/Fe] II	3.13	0.00	0.05	−0.03	0.06	HFS
[Ti/Fe] I	5.00	0.03	0.03	0.01	0.06	
[Ti/Fe] II	5.07	0.12	0.05			
[V/Fe] I	3.97	−0.08	0.04	−0.16	0.08	HFS
[Cr/Fe] I	5.67	−0.15	0.05	−0.13	0.08	
[Mn/Fe] I	5.34	0.00	0.02			HFS
[Ni/Fe] I	6.28	0.04	0.04	0.07	0.03	
[Ba/Fe] II	2.18	0.14	0.08	0.30	0.09	

5853.69, 6141.75, and 6496.91 Å. These lines yield abundances that agree well, with a typical rms of 0.12 dex for any given star. The star-to-star variations (0.08 dex) are due to the uncertainties in atmospheric parameters, especially in $T_{\rm eff}$ and $v_{\rm t}$. We have only a single Ba line (at 6141.75 Å) in the GIRAFFE spectra. There is an offset between the Ba abundances measured in the two types of spectra, which can be explained by differences in the EWs, however. The EWs of the 6141 Å are larger for GIRAFFE than for UVES stars of similar atmospheric parameters, most probably because of an unresolved blend with Ni I and Si I in the lower resolution spectra. The contaminant-line contributions to the GIRAFFE Ba lines seems confirmed by estimates of their fractions to the total EW of the blended Ba II feature.

Given the strength of the Ba II lines, which are always saturated, Ba is a difficult element to measure. However, three stars of the faint sample (1082, 1357, and 2170) show a very high Ba abundance; all three have RVs compatible with cluster membership. The first is the most convincing case suggestive of an s-process-enriched "Barium star". Not only is its Ba line much stronger than in stars of similar atmospheric parameters and normal Ba abundance (see Fig. 8), it also shows a clear La II line
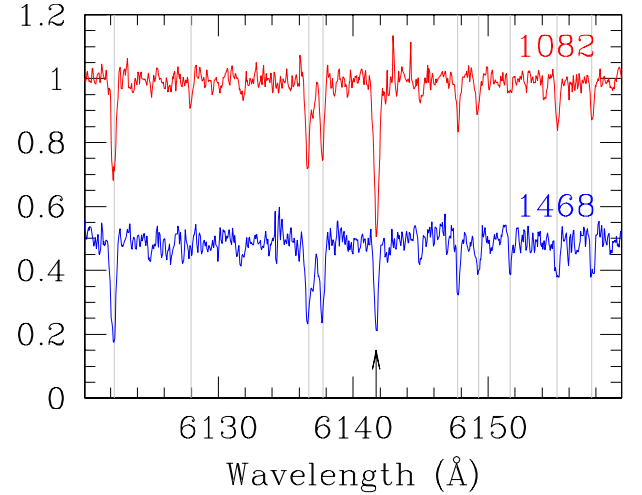
Fig. 8. Comparison of the Ba II 6141.7 Å line (indicated by an arrow) in the Ba-star 1082 and in the star 1468, of very close atmospheric parameters, as confirmed by the similarity of the other lines seen here (Ca, Ni, two Fe I, Fe I+Fe II, Fe II, Fe I, Na, and Si, from left to right and indicated by grey lines). The spectra are shifted for clarity.

at 6320.4 Å, not detected in other, similar objects. Star 1082 is brighter than expected from a single star at the TO and could be a blue straggler; the high Ba could be due to mass transfer in a binary system. Since stars on the main sequence have only a tiny convective envelope, it does not need to have accreted a lot of mass to explain the higher Ba abundance; this would be possible even in a wide system and this would explain why its RV is not discrepant from the cluster' average value.

4.1. Na and O abundances

The main goal of our study was determining the Na and O abundances in Be 39 members to see whether they show an intrinsic star-to-star scatter or even an anti-correlation, the main spectroscopic signature of multiple populations in clusters.

We measured oxygen abundances from the [O I] line using spectrum synthesis. We considered the Ni I contamination of the line (see e.g., Carretta et al. 2007), as well as the coupling of O and C expected in cool stars. The dissociation equilibrium was computed assuming [C/Fe] = −0.2 and [N/Fe] = 0.5, which are typical values for red giants in old OCs (see Mikolaitis et al. 2012). To estimate the sensitivity of our O abundances to this assumption, we note that they would be higher by ∼0.05 dex for RC stars and by 0.11 dex for stars at the tip of the RGB had we instead assumed [C/Fe] = 0.

Only the Na doublet at 6154–6160 Å was used to measure sodium abundances since the Na D and 5686–5690 lines appear only in the UVES spectra and are too strong at this metallicity. These abundances were corrected for NLTE effects using the relation by Lind et al. (2011)[3]. We interpolated their corrections with the quadratic relation $A_{\rm NLTE} − A_{\rm LTE} = −0.088 + 0.00076394 \times EW − 0.0000144444 \times EW^2$, valid for $EW <$ 150 mÅ (that is, all Na lines in our stars). The [Na/Fe] ratios (see Table 3) were then computed assuming [Fe/H] = −0.23 for UVES stars and –0.18 for GIRAFFE stars.

---

[3] We generally use the Gratton et al. (1999) corrections in our works on GCs; however, given the much higher metallicity of Be 39, we preferred to adopt the Lind et al. (2011) method. This does not mean that we need to revise all our Na abundances, since the older NLTE corrections were computed for the metallicity regime of GCs.
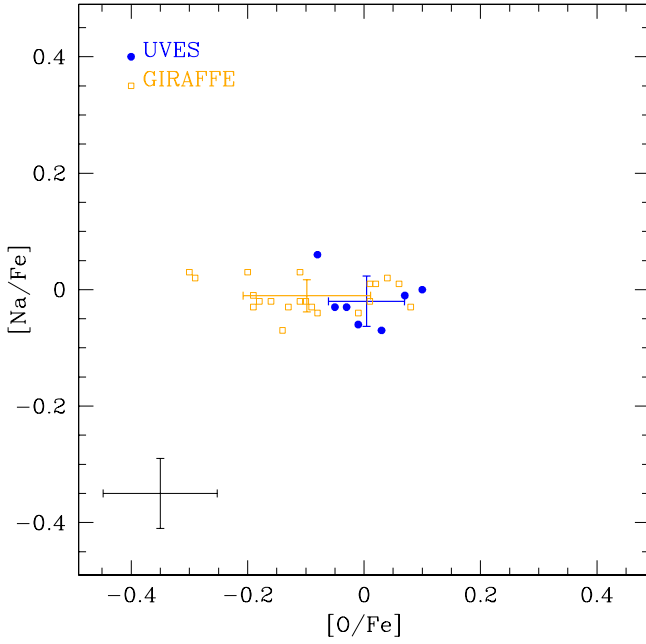
Fig. 9. Na and O distribution for the UVES (filled blue points) and the bright GIRAFFE (open orange squares). The rms in O and Na are shown by errorbars of different colour. The expected errors on O and Na abundances (see Table 4) are shown as black errorbars in the left lower corner of the plot; they are comparable to the observed rms.

Neither O nor Na abundances show any significant trend with $T_{\rm eff}$ or $\log g$ (see lower panels of Fig. 6). As apparent from Fig. 9 and from the very small scatters associated both to the O and Na values (Table 5), Be 39 is very uniform in these elements as well. The star-to-star scatter is completely explained by the associated internal errors; the only effect mimicking a relation between O and Na is the small offset between the UVES and GIRAFFE samples. Even with all the caveats already presented, this is a solid result: Be 39 is a normal OC, without any signature of the Na-O anti-correlation, which is the typical "tag" for a genuine GC (Carretta et al. 2010).

4.2. Comparison with Friel et al. (2010)

Friel et al. (2010) observed two RC and two bright RGB stars using the echelle spectrograph on the KPNO 4m telescope. We give the data for the three objects in common with our study in Table 6; two of them were observed with UVES fibres, one with GIRAFFE. The resolution of their spectra is $R \sim 28\,000$, intermediate between our GIRAFFE and UVES spectra, the wavelength coverage is $\lambda\lambda = 4800-8100$ Å, and the S/N is always high, between 70 and 115. Friel and coworkers noted that one star (WEBDA ID 2619, or 2130 for Kassis et al. 1997, adopted as our ID) is probably a binary, combining their data and the RV measured by Frinchaboy et al. (2006), differing by about 10 km s^{-1}. We do not see any strong indication of an RV change in our data, but the average RV is about 1.5 km s^{-1} lower than theirs. A similar behaviour is shown by star 1435/1139, again with our RV lower by about 6 km s^{-1} but no strong signature of RV variation (only one discrepant value in our six measures). We therefore define those two stars as probable binaries.

Table 6 displays a direct comparison of the Friel et al. (2010) atmospheric parameters and ours; they generally agree well. We also compared our EWs with theirs; the agreement is excellent, with our EWs slightly smaller. We find

Table 6. Comparison with Friel et al. (2010) for two UVES stars and one GIRAFFE star.

Star	$T_{\rm eff}$	$\log g$	$v_{\rm t}$	RV	ID	$T_{\rm eff}$	$\log g$	$v_{\rm t}$	RV	U/G
	Friel et al. (2010)					This paper				
2055	4450	1.8	1.5	57.5	1657	4399	2.10	1.54	57.5	U
2619	4750	2.2	1.5	60.0	2130	4740	2.43	1.44	58.5	U
1435	4750	2.2	1.5	62.8	1139	4659	2.46	1.43	56.9	G

Element	Abu	rms	Abu	rms	Friel+10
	UVES		Giraffe		
[Fe/H] I	−0.23	0.04	−0.18	0.06	−0.21
[O/Fe] I	0.03	0.07	−0.12	0.11	0.02
[Na/Fe] I	−0.02	0.04	−0.01	0.03	0.09
[Mg/Fe] I	0.20	0.02	0.22	0.05	0.19
[Al/Fe] I	0.05	0.03			0.20
[Si/Fe] I	0.14	0.05	0.14	0.05	0.20
[Ca/Fe] I	0.10	0.05	0.15	0.08	0.01
[Ti/Fe] I	0.06	0.03	−0.01	0.06	0.03
[Ti/Fe] II	0.15	0.05			−0.09
[Cr/Fe] I	−0.13	0.05	−0.13	0.08	0.06
[Ni/Fe] I	0.07	0.04	0.05	0.03	−0.06

$EW_{\rm UVES} = 0.992(\pm0.019) \times EW_{\rm Friel} - 3.86$ mÅ (with rms = 0.64 mÅ, over 102 lines) and $EW_{\rm GIRAFFE} = 1.030(\pm0.046) \times EW_{\rm Friel} - 1.1$ mÅ (with rms = 0.76 mÅ, over 26 lines).

A detailed comparison of the two analyses is beyond the scope of our paper. We only note that the derived abundances agree well (see Table 6), especially for iron and the α-elements. We also recall that we corrected the Na abundances for NLTE, while Friel and collaborators did not, since these corrections are small for such high-metallicity, warm stars. Finally, we do not provide here any comparison with the properties of other clusters, or discuss the radial abundance distribution. This is outside the main goal of our study; moreover, the abundances are so similar to those derived by Friel et al. (2010) that all considerations and conclusions of these authors apply.

5. Summary and conclusions

We presented the abundance analysis of the high mass, old OC Be 39. The high-resolution spectra of more than 100 stars, obtained with VLT/FLAMES, permitted us to isolate about 70 cluster members. With the advent of surveys targeting large numbers of stars in large and significant sets of clusters (e.g., the Gaia-ESO Survey, recently started on VLT/FLAMES, see Gilmore et al. 2012), comparable samples will become more common, but this is presently the largest sample of stars in this particular cluster and one of the largest in general. The membership information was used to determine updated cluster parameters (age, reddening, and distance). About one half of the stars were analysed to determine metallicity and detailed elemental abundances. We confirmed the slightly sub-solar metallicity of Be 39 ([Fe/H] = −0.2) and the very small scatter around the average abundances for all elements measured (Fe, O, Na, Al, α-, iron-peak, and heavy elements). This is interesting also in the context of cluster and disc formation mechanisms and disc chemical evolution.

The observations were optimised to look in particular for possible star-to-star variations in O and Na, which are indicative of the existence of multiple populations in this cluster, in analogy to what is is found for the higher mass, older GCs. No such scatter or anti-correlation was found; and we conclude that Be 39 is a normal, homogeneous, single-population cluster.

References

Alonso, A., Arribas, S., & Martínez-Roger, C. 1999, A&AS, 140, 261
Bellazzini, M., Perina, S., Galleti, S., et al. 2008, Mem. Soc. Astron. It., 79, 663
Bragaglia, A. 2012, AAS Meeting Abstracts, 220, 102.03
Bragaglia, A., & Tosi, M. 2006, AJ, 131, 1544
Bragaglia, A., Carretta, E., Gratton, R. G., et al. 2001, AJ, 121, 327
Carretta, E., Bragaglia, A., & Gratton, R. G. 2007, A&A, 473, 129
Carretta, E., Bragaglia, A., Gratton, R. G., et al. 2009a, A&A, 505, 117
Carretta, E., Bragaglia, A., Gratton, R., & Lucatello, S. 2009b, A&A, 505, 139
Carretta, E., Bragaglia, A., Gratton, R. G., et al. 2010, A&A, 516, A55
Carretta, E., Bragaglia, A., Gratton, R., D'Orazi, V., & Lucatello, S. 2011, A&A, 535, A121
Carretta, E., Bragaglia, A., Gratton, R. G., Lucatello, S., & D'Orazi, V. 2012, ApJ, 750, L14
Cohen, J. G. 2004, AJ, 127, 1545
de Silva, G. M., Gibson, B. K., Lattanzio, J., & Asplund, M. 2009, A&A, 500, L25
Dias, W. S., Alessi, B. S., Moitinho, A., & Lépine, J. R. D. 2002, A&A, 389, 871
Friel, E. D. 1995, ARA&A, 33, 381
Friel, E. D., Janes, K. A., Tavarez, M., et al. 2002, AJ, 124, 2693
Friel, E. D., Jacobson, H. R., & Pilachowski, C. A. 2010, AJ, 139, 1942
Frinchaboy, P. M., Muñoz, R. R., Phelps, R. L., Majewski, S. R., & Kunkel, W. E. 2006, AJ, 131, 922
Geisler, D., & Villanova, S. 2012, AAS Meeting Abstracts, 220, 102.02
Geisler, D., Villanova, S., Carraro, G., et al. 2012, ApJ, 756, L40
Gilmore, G., Randich, S., Asplund, M., et al. 2012, The Messenger, 147, 25
Gratton, R. G. 1988, Rome Obs. Preprint Ser., 29
Gratton, R. G., Carretta, E., & Castelli, F. 1996, A&A, 314, 191
Gratton, R. G., Carretta, E., Eriksson, K., & Gustafsson, B. 1999, A&A, 350, 955
Gratton, R. G., Carretta, E., Claudi, R., Lucatello, S., & Barbieri, M. 2003, A&A, 404, 187
Gratton, R., Sneden, C., & Carretta, E. 2004, ARA&A, 42, 385
Gratton, R. G., Carretta, E., & Bragaglia, A. 2012, A&ARv, 20, 50
Kassis, M., Janes, K. A., Friel, E. D., & Phelps, R. L. 1997, AJ, 113, 1723
Kaluzny, J., & Richtler, T. 1989, Acta Astron., 39, 139
Kurucz, R. 1993, ATLAS9 Stellar Atmosphere Programs and 2 km s^{-1} grid, Kurucz CD-ROM No. 13, Cambridge, Mass.: Smithsonian Astrophysical Observatory
Lata, S., Pandey, A. K., Sagar, R., & Mohan, V. 2002, A&A, 388, 158
Lind, K., Asplund, M., Barklem, P. S., & Belyaev, A. K. 2011, A&A, 528, A103
Magain, P. 1984, A&A, 134, 189
Magrini, L., Sestito, P., Randich, S., & Galli, D. 2009, A&A, 494, 95
Marigo, P., Girardi, L., Bressan, A., et al. 2008, A&A, 482, 883
Martell, S. L., & Grebel, E. K. 2010, A&A, 519, A14
Martell, S. L., & Smith, G. H. 2009, PASP, 121, 577
Mikolaitis, S., Tautvaisiene, G., Gratton, R., Bragaglia, A., & Carretta, E. 2012, A&A, 541, A137
Pasquini, L., Avila, G., Blecha, A., et al. 2002, The Messenger, 110, 1
Ramírez, I., & Meléndez, J. 2005, ApJ, 626, 465
Robin, A. C., Reylé, C., Derrière, S., & Picaud, S. 2003, A&A, 409, 523
Sbordone, L., Bonifacio, P., Marconi, G., Buonanno, R., & Zaggia, S. 2005, A&A, 437, 905
Sbordone, L., Bonifacio, P., Buonanno, R., et al. 2007, A&A, 465, 815
Sbordone, L., Salaris, M., Weiss, A., & Cassisi, S. 2011, A&A, 534, A9
Tautvaišienė, G., Wallerstein, G., Geisler, D., Gonzalez, G., & Charbonnel, C. 2004, AJ, 127, 373
Yong, D., Carney, B. W., & Friel, E. D. 2012, AJ, 144, 95

Table 2. Information on the observed stars.

ID$_{Kassis}$	ID$_{WEBDA}$	RA (hh mm ss)	Dec (dd pp ss)	V	B − V	V − I	S/N	RV km s^{-1}	Notes
			UVES sample						
1256	1587	7 46 52.49	−4 41 14.61	14.426	1.223	1.239	123	57.04	
1407	1767	7 46 50.77	−4 41 28.96	14.166	1.24	1.147	125	57.58	a
1657	2055	7 46 47.60	−4 39 56.35	13.995	1.291	1.495	164	57.58	*
2130	2619	7 46 41.44	−4 39 8.28	14.417	1.202	1.285	103	58.59	*, bin?
2144	2634	7 46 41.25	−4 40 57.13	14.377	1.221	1.179	104	57.56	
2262	2784	7 46 39.27	−4 37 54.30	14.199	1.245	1.203	167	55.76	
2376	2939	7 46 37.15	−4 40 11.39	14.075	1.202	1.196	112	57.31	
			GIRAFFE, bright sample						
1125	1411	7 46 54.42	−4 41 28.11	13.531	1.496	1.60	1124	58.76	b
892	1122	7 46 58.01	−4 33 54.96	14.107	1.288	1.048	271	58.20	
281	348	7 47 10.76	−4 36 25.80	14.856	1.254	1.246	147	58.25	
2089	2573	7 46 42.05	−4 41 5.99	14.740	1.218	1.236	131	58.01	
1374	1725	7 46 51.15	−4 40 29.32	14.783	1.293	1.292	172	60.48	
1139	1435	7 46 54.15	−4 38 58.13	14.359	1.13	1.246	205	56.94	*, a, bin?
2284	2817	7 46 38.98	−4 41 56.34	14.828	1.22	1.201	143	59.04	a
1068	1349	7 46 55.10	−4 39 27.20	15.214	1.227	1.276	157	56.20	
591	755	7 47 3.79	−4 39 14.45	14.465	1.252	1.20	185	57.31	b
802	1019	7 46 59.82	−4 41 48.04	14.375	1.209	1.29	158	56.68	b
1447	1817	7 46 50.09	−4 36 0.38	14.322	1.175	1.195	211	56.95	
984	1248	7 46 56.54	−4 43 51.11	14.335	1.399	1.203	243	57.59	
537	680	7 47 4.94	−4 35 42.37	15.497	1.137	1.161	99	59.20	
618	782	7 47 3.32	−4 39 43.48	15.810	1.204	1.245	71	57.99	
1411	1770	7 46 50.82	−4 46 57.77	14.096	1.257	1.230	223	57.67	
1363	1709	7 46 51.21	−4 36 3.53	15.494	1.124	1.152	114	58.08	
1547	1923	7 46 49.12	−4 41 55.64	15.518	1.18	1.333	106	59.15	a
1057	1333	7 46 55.20	−4 36 51.16	15.889	1.057	1.103	81	57.86	
1310	1637	7 46 51.91	−4 33 37.88	15.818	1.033	1.146	64	59.43	
773	978	7 47 0.14	−4 33 26.07	15.888	1.039	1.052	99	58.29	
2088	2575	7 46 42.05	−4 39 19.44	13.004	1.739	1.70	97	59.42	b
11	12	7 47 17.80	−4 44 14.56	14.487	1.424	1.297	97	65.05	NM?
			GIRAFFE, faint sample						
2373	2934	7 46 37.263	−4 36 51.93	17.125	0.998	1.074	31	61.79	M?
1761	2189	7 46 46.291	−4 40 3.97	16.582	1.108	1.145	69	59.92	
2380	2947	7 46 37.087	−4 39 7.22	16.740	1.017	1.045	61	56.59	
1582	1966	7 46 48.553	−4 39 9.17	16.725	1.060	1.143	41	57.14	
1058	1340	7 46 55.239	−4 40 12.56	17.085	0.956	0.970	63	57.60	
2033	2517	7 46 42.689	−4 40 2.96	16.986	0.954	1.074	24	53.68	M?
2184	2681	7 46 40.735	−4 41 56.60	16.906	0.930	0.775	46	56.06	
2962	3704	7 46 24.123	−4 40 14.79	16.870	0.896	0.955	33	58.21	
730	920	7 47 1.059	−4 39 53.68	16.977	0.903	1.003	46	58.30	
1687	2095	7 46 47.194	−4 37 32.09	16.806	0.853	0.930	47	58.45	
2177	2672	7 46 40.815	−4 37 21.15	16.781	0.819	0.939	43	57.05	
2001	2478	7 46 43.384	−4 45 36.69	17.064	0.762	0.869	43	57.96	
1962	2429	7 46 43.968	−4 44 32.96	16.807	0.817	0.887	49	58.42	
2057	2540	7 46 42.484	−4 41 28.45	16.792	0.784	0.8	69	58.14	b
1836	2274	7 46 45.586	−4 42 47.01	16.803	0.778	0.893	64	57.86	
2050	2531	7 46 42.424	−4 35 0.61	16.878	0.648	0.801	39	56.68	
2415	2988	7 46 36.530	−4 39 48.40	16.775	0.703	0.792	33	57.58	
1280	1609	7 46 52.274	−4 42 31.59	17.192	0.766	0.871	32	57.75	
2626	3262	7 46 32.435	−4 39 48.32	17.491	0.683	0.802	14	57.39	
1470	1836	7 46 49.917	−4 41 44.79	16.979	0.66	0.753	78	58.20	a
2913	3644	7 46 25.315	−4 36 38.04	17.179	0.695	0.733	35	58.84	
1082	1366	7 46 55.069	−4 45 25.03	16.872	0.777	0.833	61	57.47	
1468	1845	7 46 49.827	−4 38 52.36	17.191	0.716	0.830	27	58.67	
2000	2475	7 46 43.369	−4 43 19.94	17.160	0.690	0.75	31	58.00	b
2170	2665	7 46 40.910	−4 38 4.75	17.564	0.702	0.797	27	58.66	
2948	3685	7 46 24.532	−4 41 25.96	17.420	0.740	0.835	20	58.77	
1176	1490	7 46 53.715	−4 43 30.62	17.026	0.967	0.835	34	58.13	
2018	2498	7 46 42.958	−4 34 53.38	16.909	0.661	0.785	50	59.22	
1126	1412	7 46 54.419	−4 40 57.18	17.220	0.732	0.876	64	58.97	
2460	3050	7 46 35.604	−4 42 9.83	17.089	0.704	0.838	42	58.58	

Notes. ID$_{Kassis}$ is taken from Kassis et al. (1997); ID$_{WEBDA}$ is the identification in the WEBDA. [*] Friel et al. (2010); a: B − V colour modified (see text); b: V − I colour modified (see text).

Table 2. continued.

ID$_{\text{Kassis}}$	ID$_{\text{WEBDA}}$	RA (hh mm ss)	Dec (dd pp ss)	V	B − V	V − I	S/N	RV km s^{-1}	Notes
1544	1920	7 46 49.137	−4 40 52.57	17.018	0.65	0.8	50	58.92	a, b
1432	1800	7 46 50.319	−4 39 40.50	17.205	0.728	0.75	26	58.34	b
699	881	7 47 1.653	−4 42 16.54	16.789	0.606	0.713	35	59.62	
1357	1704	7 46 51.313	−4 38 48.62	17.098	0.720	0.833	47	61.13	M?
1422	1786	7 46 50.441	−4 37 31.57	17.383	0.676	0.855	42	55.76	
1534	1910	7 46 49.143	−4 36 24.08	17.402	0.693	0.822	32	57.27	
866	1097	7 46 58.556	−4 40 59.95	17.215	0.708	0.848	39	58.33	
2170	2665	7 46 40.910	−4 38 4.75	17.564	0.702	0.797	68	58.66	
Binaries / not analysed									
954	1202	7 46 56.936	−4 36 13.28	15.318	1.093	1.209			
727	914	7 47 1.217	−4 42 45.20	15.570	1.147	1.158			
517	656	7 47 5.412	−4 39 41.65	16.415	1.214	1.317			
2976	3723	7 46 23.872	−4 42 50.22	16.589	0.945	0.907			
1252	1583	7 46 52.513	−4 39 23.24	17.121	0.720	0.870			
1675	2076	7 46 47.483	−4 41 45.58	16.884	0.726	0.752			
1926	2377	7 46 44.491	−4 41 37.83	16.698	0.853	0.772			
1952	2414	7 46 44.071	−4 39 33.14	16.678	0.775	0.900			
Non members / not analysed									
110	133	7 47 15.241	−4 38 31.00	15.956	0.958	1.152		102.43	
24	31	7 47 17.435	−4 42 34.78	14.613	1.209	1.195		101.53	
408	514	7 47 7.862	−4 44 48.50	14.600	1.106	1.147		32.58	
430	546	7 47 7.263	−4 43 0.40	14.223	1.333	1.298		83.41	
1098	1382	7 46 54.829	−4 43 18.48	16.000	1.280	1.422		3.03	
1114	1398	7 46 54.590	−4 44 17.30	15.920	1.237	1.268		13.24	
1356	1705	7 46 51.422	−4 45 9.83	15.403	1.178	1.232		42.59	
2290	2820	7 46 39.021	−4 46 57.33	15.959	1.440	1.584		33.51	
3090	3889	7 46 20.726	−4 38 4.49	14.338	1.191	1.214		85.58	
2832	3530	7 46 27.182	−4 34 28.11	17.046	0.498	0.701		79.10	
2560	3180	7 46 33.644	−4 34 35.33	17.024	0.947	0.857		63.05	
2278	2805	7 46 39.015	−4 35 23.01	17.067	0.678	0.809		75.85	
2151	2643	7 46 41.099	−4 35 7.35	16.751	0.578	0.730		108.66	
1833	2267	7 46 45.461	−4 32 53.31	16.950	0.931	0.941		26.91	
1762	2186	7 46 46.232	−4 37 52.82	16.877	0.671	0.869		37.43	
2324	2865	7 46 38.414	−4 40 6.52	16.993	0.720	0.847		36.19	
1040	1313	7 46 55.437	−4 38 5.71	17.646	0.750	0.860		71.27	
1448	1819	7 46 50.080	−4 36 41.64	17.098	0.735	0.832		48.77	
761	963	7 47 0.441	−4 36 59.03	16.756	0.734	0.822		68.09	
151	188	7 47 14.226	−4 36 11.67	17.060	0.753	0.820		5.60	
87	107	7 47 15.636	−4 37 28.78	17.195	0.825	0.886		88.90	
500	630	7 47 5.825	−4 42 15.99	16.627	0.944	1.023		137.52	
115	141	7 47 15.258	−4 44 42.29	16.798	0.766	0.872		18.11	
266	328	7 47 11.409	−4 42 7.11	17.086	0.629	0.764		66.15	
160	197	7 47 14.340	−4 47 20.31	16.565	0.776	0.905		77.81	
438	558	7 47 7.122	−4 46 37.33	16.274	1.056	1.096		129.21	
239	296	7 47 12.044	−4 44 28.53	16.909	0.654	0.797		90.03	
1334	1675	7 46 51.778	−4 44 25.76	17.222	0.827	0.939		40.21	
670	848	7 47 2.233	−4 43 33.16	17.472	0.900	1.007		38.78	
2232	2737	7 46 39.965	−4 45 51.50	16.997	0.793	0.919		83.98	
2231	2735	7 46 39.989	−4 46 50.06	17.158	0.900	0.902		91.74	
1321	1656	7 46 51.940	−4 43 13.64	16.757	1.021	0.872		39.24	
2259	2780	7 46 39.512	−4 46 16.45	17.089	0.859	0.922		73.54	
2688	3339	7 46 30.808	−4 43 17.74	16.771	0.678	0.787		32.59	
2820	3518	7 46 27.473	−4 41 6.48	16.927	1.176	1.234		28.32	
3100	3902	7 46 20.581	−4 42 46.21	16.955	1.145	0.815		1.95	
3024	3801	7 46 22.176	−4 41 17.16	16.560	1.177	1.200		8.27	
2776	3453	7 46 28.570	−4 38 35.42	17.343	0.593	0.744		47.52	
2644	3283	7 46 32.096	−4 38 1.67	17.129	0.561	0.711		74.72	
3130	3942	7 46 19.936	−4 36 52.16	17.063	0.749	0.894		76.67	
3150	3964	7 46 19.411	−4 35 51.95	16.976	0.826	0.570		64.35	
2033	2517	7 46 42.689	−4 40 2.96	16.986	0.954	1.074		53.68	
643	813	7 47 2.859	−4 40 58.92	16.880	0.781	0.899		58.84	

Table 3. Stellar parameters, number of lines, Fe, Na, and O abundances and errors.

Star	$T_{\rm eff}$ (K)	$\log g$ (dex)	v_t km s^{-1}	Nr	[Fe/H]I	rms	Nr	[Fe/H]II	rms	[O/Fe]	err	Nr	[Na/Fe]	rms
						UVES sample								
1256	4751	2.45	1.43	48	–0.19	0.07	10	–0.20	0.09	–0.03		2	–0.03	0.00
1407	4801	2.42	1.44	50	–0.24	0.07	10	–0.33	0.08	–0.08		2	0.06	0.02
1657	4399	2.10	1.54	44	–0.28	0.08	8	–0.30	0.12	0.03		2	–0.07	0.03
2130	4740	2.43	1.44	47	–0.21	0.07	10	–0.22	0.07	0.07		2	–0.01	0.01
2144	4752	2.35	1.46	50	–0.23	0.08	10	–0.28	0.07	–0.05		2	–0.03	0.01
2262	4708	2.27	1.49	48	–0.25	0.06	10	–0.29	0.07	–0.01		2	–0.06	0.01
2376	4679	2.47	1.42	46	–0.18	0.07	10	–0.14	0.09	0.10		2	0.00	0.01
					GIRAFFE, bright sample									
1125	4150	1.74	1.66	8	–0.23	0.16	3	–0.19	0.22	–0.08	0.01	2	–0.04	0.00
892	4536	2.41	1.44	8	–0.20	0.12	3	–0.23	0.13	0.06	0.05	2	0.01	0.02
281	4599	2.60	1.38	8	–0.20	0.11	3	–0.20	0.15	–0.11	0.06	2	–0.02	0.01
2089	4609	2.58	1.39	8	–0.18	0.08	3	–0.25	0.12	–0.10	0.06	2	–0.02	0.01
1374	4622	2.52	1.41	8	–0.17	0.11	3	–0.21	0.08	–0.09	0.06	2	–0.03	0.08
1139	4659	2.46	1.43	8	–0.16	0.11	3	–0.09	0.12	–0.19	0.05	2	–0.01	0.02
2284	4692	2.65	1.37	8	–0.14	0.12	3	–0.20	0.08	–0.11	0.07	2	0.03	0.02
1068	4705	2.74	1.34	8	–0.24	0.09	3	–0.24	0.15	–0.13	0.08	2	–0.03	0.02
591	4706	2.45	1.43	8	–0.17	0.11	3	–0.23	0.13	–0.18	0.05	2	–0.02	0.01
802	4728	2.41	1.44	8	–0.17	0.11	3	–0.20	0.09	–0.19	0.05	2	–0.03	0.01
1447	4751	2.46	1.43	8	–0.15	0.12	3	–0.18	0.10	–0.16	0.05	2	–0.02	0.01
984	4768	2.33	1.47	12	–0.19	0.11	3	–0.25	0.13	–0.29	0.04	2	0.02	0.02
537	4779	2.97	1.26	8	–0.23	0.12	3	–0.07	0.12	0.01	0.13	2	–0.02	0.04
618	4824	3.01	1.25	8	–0.16	0.12	3	–0.18	0.15	–0.01	0.13	2	–0.04	0.06
1411	4844	2.30	1.48	12	–0.20	0.11	3	–0.29	0.08	–0.30	0.04	2	0.03	0.01
1363	4848	2.98	1.26	8	–0.17	0.11	3	–0.29	0.11	0.04	0.13	2	0.02	0.03
1547	4765	2.84	1.31	7	–0.17	0.11	3	–0.24	0.15	–0.20	0.10	2	0.03	0.10
1057	4922	3.21	1.19	8	–0.17	0.13	3	–0.21	0.14	0.01	0.19	2	0.01	0.03
1310	4958	3.17	1.20	8	–0.17	0.08	3	–0.27	0.18	0.02	0.18	2	0.01	0.02
773	4934	3.25	1.17	8	–0.17	0.10	3	–0.35	0.17	0.08	0.20	2	–0.03	0.06
2088	4043	1.28	1.81	9	–0.37	0.21	3	–0.28	0.26	–0.14	0.01	2	–0.07	0.07
11	4387	2.32	1.47	8	–0.02	0.18	3	–0.02	0.18	–0.15	0.04	2	0.10	0.02